Extended micromagnetic model for the detection of superparamagnetic labels using a GMR vortex sensor

Journal of Physics Communications

PAPER

Extended micromagnetic model for the detection of superparamagnetic labels using a GMR vortex sensor

Lukas Wetterau[1], **Claas Abert**[2], **Dieter Suess**[2], **Manfred Albrecht**[3] and **Bernd Witzigmann**[4]

[1] Computational Electronics and Photonics and CINSaT, University of Kassel, Kassel, Germany
[2] Physics of Functional Materials, University of Vienna, Vienna, Austria
[3] Institute of Physics, University of Augsburg, Augsburg, Germany
[4] Department of Electrical Engineering, University of Erlangen-Nürnberg, Erlangen, Germany

E-mail: lukas.wetterau@uni-kassel.de

OPEN ACCESS

RECEIVED
5 July 2021

REVISED
20 July 2021

ACCEPTED FOR PUBLICATION
23 July 2021

PUBLISHED
2 August 2021

Keywords: microfluidic lab-on-a-chip devices, micromagnetic simulations, superparamagnetic labels

Abstract

A self-consistent micromagnetic model is proposed for simulating interactions between a superparamagnetic label particle and a low-noise GMR vortex sensor, focusing on most common operations such as label detection and saturation. For this purpose, we evaluate the combined action of vortex stray field and the applied external field.

By solving the Landau–Lifshitz-Gilbert equation we find that a superparamagnetic label with a diameter of 60 nm can be successfully detected by a magnetic vortex structure assisted with an external magnetic field of 100 mT. Subsequently, the self-consistent spin diffusion model is applied to calculate electric response of a standard low-noise GMR vortex sensor to the presence of magnetically-saturated label. It is shown that the stray field of the activated label produces a detectable potential difference in the GMR sensor of 27.1 to 27.8 mV, the magnitude of which depends on location of the label with respect to the sensor surface.

1. Introduction

The development of microfluidic systems improving the analysis and performance of Point-of-Care (POC) diagnosis is a topical issue in biomedical research [1–3]. Especially, a microfluidic system based on magnetic field interaction is a promising technology that offers high sensitivity and specificity [4]. Since magnetic signals caused by plenty of molecules (DNA, proteins, viruses and cells) range from fT to nT, magnetic-based microfluidic systems utilize bio-functionalized labels to enhance magnetostatic interaction [5]. Here, the magnetic stray field of the label is used to enable efficient separation [6], safe transportation [7], and reliable detection [8].

The use of magnetic stray fields prevents interference issues, which appear in technologies that employ light absorption to detect fluorescent signals [9]. Furthermore, it allows the usage of already developed CMOS techniques for the design of the sensing unit with direct electronic readout [9]. For this purpose, magnetoresistive sensors are ideal candidates, since they are already part of many sensing applications and well investigated concerning an application in a microfluidic system [8].

However, the detection and quantification of bio-functionalized labels requires a sensor element that offers a high signal-to-noise ratio and a linear sensor response. In this context, spin-valve structures, including a magnetic vortex structure, were introduced, reducing the magnetic noise of the giant magnetoresistance (GMR) response due to a vanishing phase noise [10]. In general, magnetic vortex structures exhibit a flux closure state of the magnetization due to the competition of the exchange energy and the demagnetization energy [11]. In micron-sized circular disks with a specific aspect ratio, the magnetization curls up, leading to an out-of-plane magnetization in the center, which is called the vortex core [12]. An external field shifts the vortex core linearly and the classical hysteresis loop changes to a linear loop between the positive and the negative vortex nucleation field. This vortex shift will lead to resistance changes in a typical GMR spin-valve if the stack's magnetic free layer

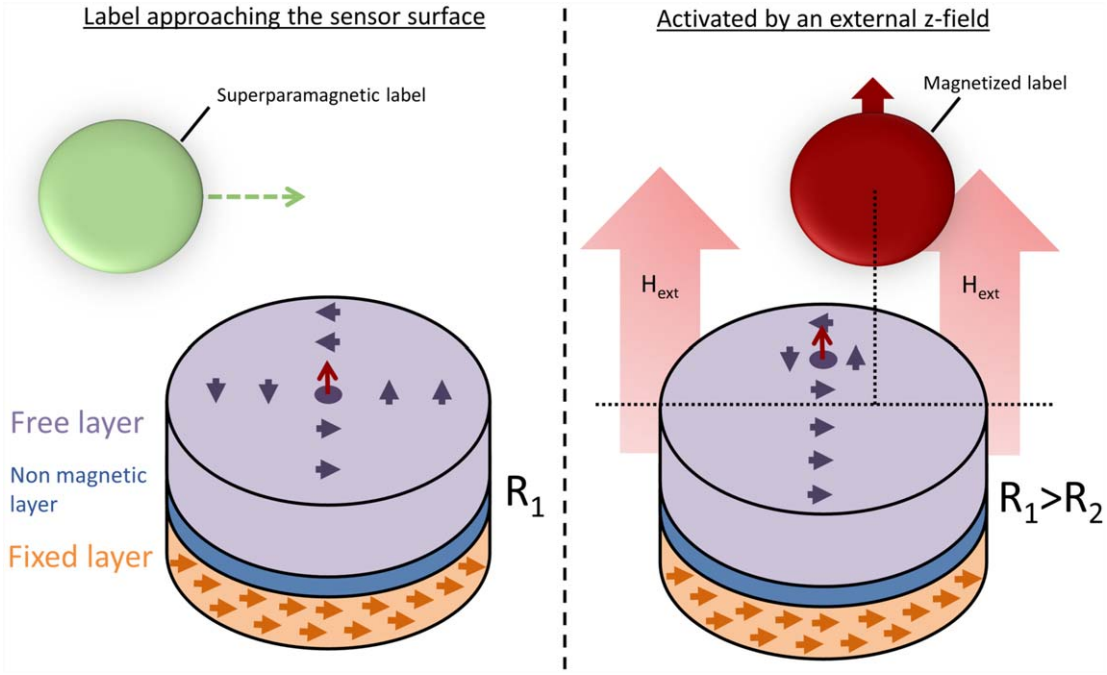

Figure 1. Sketch of the simulated sensor concept. When the label approaches the sensor element, the external z-field is already turned on or switched in specific frequency to activate the stray field of the superparamagnetic label. As a result, the magnetization of the label aligns in the z-direction and label shifts change the magnetization configuration of the free layer and thus the resistance of the layer stack.

consists of such a vortex structure [9]. Here, the magnetization orientation to the antiferromagnetically fixed layer changes, which in turn leads to resistance changes compared to the initial configuration [10].

Ferromagnetic and superparamagnetic labels are able to generate magnetic stray fields, which can be detected by electrical output of a GMR spin-valve sensor. Although ferromagnetic labels are useful for a number of applications where a permanent magnetic moment is required, they are prone of agglomeration [13]. This hinders an efficient separation and possibly elicits embolism in in-vivo applications [13]. Additionally, several essential molecules are assigned to the nanometer range, where most suitable labels exhibit superparamagnetic properties as critical diameters usually smaller than 100 nm are reached [14]. In contrast to ferromagnetic labels, superparamagnetic labels only provide magnetic moments in a certain temperature range or in the presence of an external field [14]. In this case, the spins stop flipping randomly, and a net magnetic moment appears [14]. Consequently, this property can be exploited to avoid label agglomeration in a microfluidic channel. As outlined in figure 1, the label is guided through a microfluidic channel and reaches the sensor structure in the superparamagnetic state. Upon approaching the sensor surface, an external field is present and the magnetic moment of the label appears [15]. The arising label stray field changes the magnetization configuration of the sensor stack, which in turn changes the GMR compared to the initial configuration.

In general, the numerical simulation of a label in the superparamagnetic state calls for formulations, including thermal effects. In this context, the Landau–Lifshitz-Bloch equation is suitable, which describes the magnetization dynamics at finite temperatures [16]. However, for simulating the label detection using a GMR vortex sensor, it is desirable to exploit the self-consistent spin-diffusion model since it enables a direct calculation of the GMR depending on the stray field of the label. In our previous work, we assumed that the superparamagnetic label is saturated by an external field which allowed for the application of standard micromagnetic methods [17]. However, in order to accurately resolve the interaction of the superparamagnetic label with the vortex, the influence of the vortex stray field onto the label magnetization has to be modeled as well. In this work, we present a numerical approach that uses micromagnetics for the description of the vortex structure and a simple Langevin model for the description of the superparamagnetic label. The bidirectional stray field coupling of these two structures is resolved by means of a simple fixed point iteration which turns out to be surprisingly sufficient. The model is applied to simulate the label detection using an external field in z-direction and to test the activation of the superparamagnetic label by the out-of-plane vortex core field.

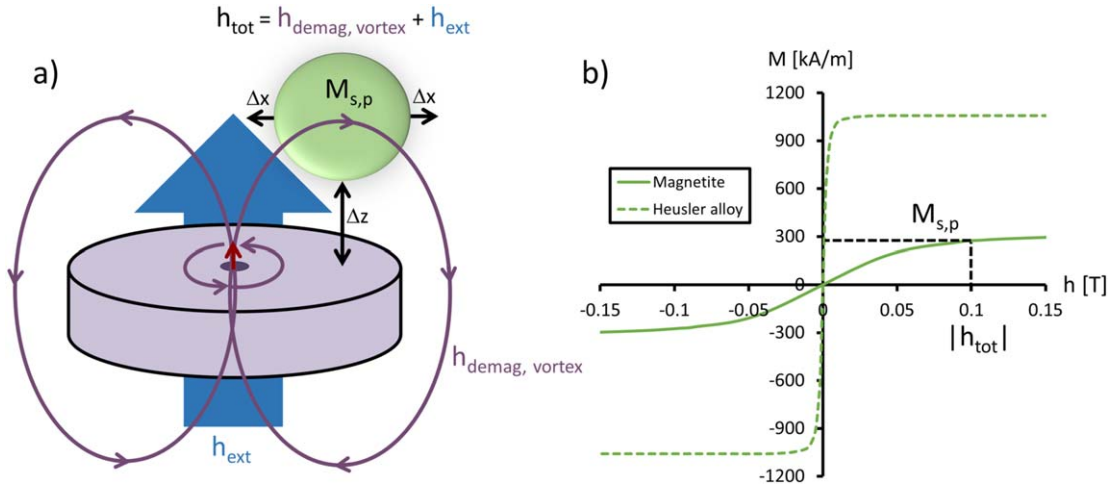

Figure 2. Evaluation of the label to simulate the superparamagnetic nature. (a) Geometry of the system used for the detection of a superparamagnetic label by a GMR sensor. The total field h_{tot} consisted of the vortex core stray field h_{vortex} and the external field h_{ext} is introduced to define the location of the label. Note that z characterizes the distance between the free layer surface and the label surface and $\Delta x/\Delta y$ the label's shift from the center of the sensor. (b) Langevin functions for magnetite [19] and Heusler alloy [20], calibrated for achieving saturation magnetization $M_{s,p}$ at the required the total field h_{tot}.

2. Simulation model and material properties

Superparamagnetism arises in small ferromagnetic particles of sizes in the nanometer range, where most nanoparticles exhibit a single-domain magnetization [14]. Induced by thermal energy, the direction of the single-domain magnetization flips randomly and the time-averaged magnetization yields zero [14]. This random flip can be stopped either at temperatures below the blocking temperature, where the random flip is decelerated, or using external fields, which exceed the material-dependent energy barrier of the nanoparticle [14]. In our simulations, thermal aspects are negligible since external fields, provided by an external source or the magnetic vortex, are intended for the activation of the label's magnetic moment.

2.1. Simulation methods

On the micron scale, the Landau–Lifshitz-Gilbert (LLG) equation describes the magnetization dynamics of a three-dimensional magnetic system as micromagnetic model. It couples an effective magnetic field $\mathbf{h}_{\text{eff}}$ to the precessional damped motion of the normalized magnetization $\mathbf{m}$. Thereby, it permits modeling of magnetic systems under the influence external fields. The LLG equation is defined by

$$\frac{\partial \mathbf{m}}{\partial t} = -\gamma(\mathbf{m} \times \mathbf{h}eff) + \alpha\left(\mathbf{m} \times \frac{\partial \mathbf{m}}{\partial t}\right) \tag{1}$$

where parameters γ and α denote the gyromagnetic ratio and the damping constant, respectively [18]. Determined by the problem setting including an external field $\mathbf{h}_{\text{ext}}$, the effective field $\mathbf{h}_{\text{eff}}$ includes

$$\mathbf{h}_{eff} = \mathbf{h}_{demag} + \mathbf{h}_{ex} + \mathbf{h}_{ext}, \tag{2}$$

where the demagnetization field $\mathbf{h}_{\text{demag}}$ accounts for the dipole-dipole interaction and the exchange field $\mathbf{h}_{\text{ex}}$ for the quantum-mechanical effect of the exchange interaction [11]. At this point, the field contributions are defined as proposed in [11] just as their corresponding boundary conditions. Accordingly, $\mathbf{h}_{\text{demag}}$ usually includes the stray field of the label and the magnetic vortex. In our extended model, the label stray field is treated separately to consider the effect of the magnetic vortex on the label, see figure 2. For this purpose, the vortex stray field is computed according to

$$\mathbf{h}_{demag,vortex} = -\nabla\left[\frac{M_{s,L}}{4\pi}\int_{\Omega_{vortex}} \frac{m \times \nabla'}{|x\text{-}x'|}dx'\right] \tag{3}$$

using the hybrid FEM/BEM method [11]. Note that Ω_{vortex} and $M_{s,L}$ describe the region and the saturation magnetization of the vortex free layer, respectively. In the next step, an average total field is computed consisting of the average vortex stray field and the applied external field both evaluated at the label position

$$\mathbf{h}_{tot} = \mathbf{h}_{demag,vortex} + \mathbf{h}_{ext}. \tag{4}$$

This total field covers all field components that affect the label and is subsequently used to determine the label's magnetization configuration. On the one hand, the magnitude of the total field is applied to the imported

Langevin function L(h) by

$$\mathbf{M}_{s,p} = \mathbf{L}(|\mathbf{h}_{tot}|) \tag{5}$$

to extract the label's saturation magnetization. On the other hand, the label's magnetization direction characterized by $\mathbf{m}_p$ is defined by the direction of the total field according to

$$\mathbf{m}_p = \frac{\mathbf{h}_{tot}}{|\mathbf{h}_{tot}|}. \tag{6}$$

The label magnetization $\mathbf{m}_p$ indicates a magnetic stray field that provokes a relaxation of the magnetic vortex. After reaching the steady state, the procedure described by equations (3) to (6) is repeated. This fixed point iteration is performed until the magnetizations of the vortex and the label converge. Here, 20 iterations are typically required for an adequate convergence.

In order to solve this micromagnetic model, the 3D finite element method is applied to the LLG equation and the corresponding energy contributions. In this regard, the magnum.fe tool provides the self-consistent spin-diffusion model to determine subsequently the GMR response of the sensor [21]. According to the general spin-diffusion approach, the excess of one spin orientation degree indicated by the magnetization direction of a ferromagnetic material is characterized by the so-called spin accumulation **s** [11]. Here, the variation of the spin accumulation degree **s** is by two orders of magnitude lower than that observed in ferromagnetic systems [21]. Accordingly, the diffusion of the spin accumulation through a state-of-the-art spin valve stack is given by the equation of motion as follows

$$\nabla \cdot \mathbf{j}_S + \frac{\mathbf{s}}{\tau_{sf}} + J\frac{\mathbf{s} \times \mathbf{m}}{\hbar} = 0. \tag{7}$$

Here, $\mathbf{j}_s$ represents the spin current caused by the motion of the spin accumulation **s** [21]. The spin current itself is directly coupled to the charge current via the electric potential **u** using $\mathbf{E} = -\Delta\mathbf{u}$ and equations (8) and (9).

$$\mathbf{j}_s = 2\beta C_0 \frac{\mu_B}{e}\mathbf{m} \otimes \mathbf{E} - 2D_0 \nabla s \tag{8}$$

$$\mathbf{j}_e = 2C_0\mathbf{E} - 2\beta' D_0 \frac{e}{\mu_0}(\nabla \mathbf{s})^T \mathbf{m} \tag{9}$$

The magnum.fe tool solves the system of equations (7)–(9) in a self-consistent fashion using boundary conditions for the spin accumulation **s**, the spin current $\mathbf{j}_e$, and the electric potential **u** [21]. At this point, J is the coupling strength and β, β' are polarization parameters, whereas the source equation (10) completes the system of equations (7)–(9) [11].

$$\nabla \cdot \mathbf{j}_e = 0 \tag{10}$$

Using the self-consistent spin-diffusion model enables the direct extraction of the electric potential **u** in simulated spintronic devices like spin-valve stacks. The simulated performance of those devices highly depends on the dimensions and the used material parameters, which are specified in the following section 2.2.

2.2. Material parameters

Concerning the design of a label, magnetite nanoparticles provide a high biocompatibility and chemical stability for biomedical applications [22–25]. Although the superparamagnetic limit depends on the synthesis technique [26], superparamagnetic properties are commonly observed below a label diameter of $d_p = 100$ nm [14]. According to [19, 27, 28], magnetite labels offer an exchange constant of $A_{ex,p} = 10$ pJ m^{-1} and a mass magnetization $M_{s;p}$ in the range of of 20 emu g^{-1} to 90 emu g^{-1} that is converted into the saturation magnetization $M_{s,p}$ assuming a density of 5.2 g cm^{-3} [29]. Depending on the applied magnetic field, the magnetization follows the Langevin function and common magnetite labels are saturated by external fields of around 100 mT [25]. Here, we extracted the Langevin function from [19] for simulating the detection of label using an external magnetic z-field.

The 60 nm large label is placed above a magnetic vortex structure that is used as the magnetic free layer of a GMR spin valve stack. In this context, theoretical and experimental investigations showed that the vortex formation strongly depends on the aspect ratio and the material parameters of the layer [12], [30–32]. Accordingly, a minimum layer thickness t_L, which depends on the layer diameter d_L and the exchange length l_{ex} of the layer, ensuring a stable vortex formation, was reported in [33]. For soft magnetic materials , it was shown that magnetic vortices arise in layers with a diameter d_L of 100 nm [33], which is required to detect labels with diameters larger than 100 nm [34]. A saturation magnetization $\mu_0 M_{s,L} = 2.0$ T [35] and an exchange constant $A_{ex,L} = 15$ pJ/m [10] characterize a CoFe alloy leading to a minimum t_L of 8.5 nm. Hence, a layer thickness $t_L = 10$ nm will ensure a stable vortex formation, as confirmed by simulations [17]. For the finite element simulations, the 3D mesh is composed of tetrahedron elements with a size of 3 nm considering the exchange lengths of the label and the free layer ($l_{ex,p} = 12.8$ nm and $l_{ex,L} = 3.1$ nm). As only the steady-state

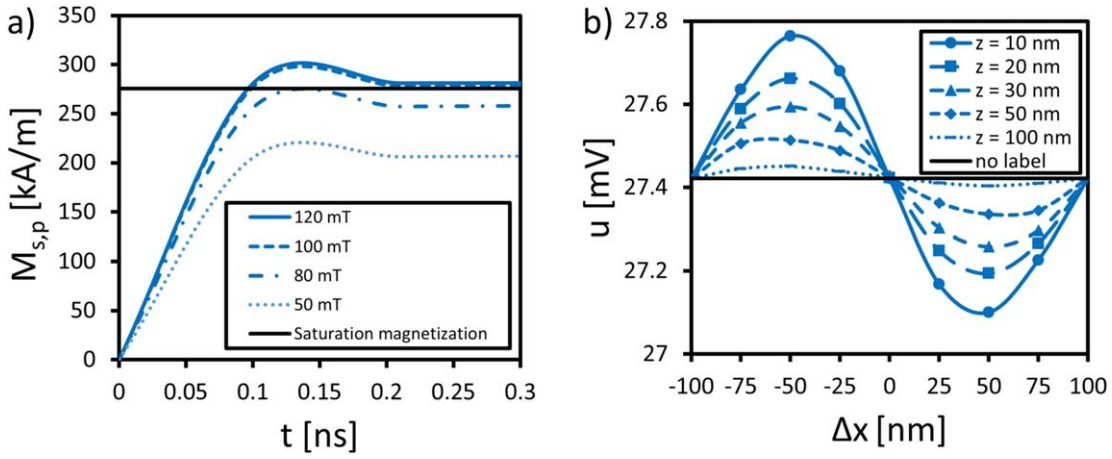

Figure 3. Simulation results for the detection of a magnetite label with a diameter of 60 nm using an external z-field ($\Delta x = 50$ nm and $z = 10$ nm). (a) Test of several external fields to verify the actual saturation field for the superparamagnetic label characterized by the Langevin function of [19]. (b) Electric potential u for several distances between the label and the sensor, depending on the horizontal offset in the x-direction.

magnetization configuration is relevant, the damping constant α_p and α_L are set to 1.0. Furthermore, the distance z between the label and the surface of the GMR sensor, as well as its horizontal offset Δx from the center of the sensor is varied. Here, Δx receives values of 25 nm, 50 nm and 75 nm, and z is varied between 10 nm and 100 nm; Δy denotes the lateral offset from the sensor center.

For the following GMR calculation, a single GMR element consisted of the CoFe free layer, a 2 nm thick Cu layer, and a 5 nm thick CoFeB fixed layer is considered. Within the self-consistent spin diffusion model represented by equations (7) to (10), the diffusion constant D_0, the spin-flip relaxation time τ_{sf}, the coupling strength J and the polarization parameters β and β' receive the values reported in [21]. The conductivity C_0 is extracted from [36–38] to be 2.5 MA/Vm for CoFe, 0.3 MA/Vm for CoFeB and 30 MA/Vm for Cu, respectively. Finally, the perpendicular-to-plane impinged electric current is $I = 8$ mA, and the magnetization of the fixed layer is pinned in the positive x-direction.

3. Results

3.1. Using an external z-field for label activation

In the first time step of the simulations, the label receives its saturation magnetization, as displayed in figure 2(a). The resulting stray field of the label coerces the magnetic vortex to start relaxation. This procedure is iterated until the system of magnetic vortex and label reaches its steady state magnetization. Due to the assumption of $\alpha = 1.0$, the steady state is achieved faster. As shown in figure 3(a), the saturation magnetization is only accomplished for external magnetic fields larger than 100 mT. This corresponds to the Langevin function that is calibrated into the simulation and thus, reproduces the superparamagnetic nature of the label concerning external magnetic fields in an adequate fashion. Here, we applied an external field of 100 mT in the z-direction.

Subsequently, the steady-state magnetization of the vortex is introduced to the the self-conistent spin diffusion model to compute the change of the sensor's GMR response. Here, the magnetization of the simulation with an external field of 100 mT is used to represent an entire saturation of the superparamagnetic label. As already demonstrated in [17], shifting the label results in an increase of the free layer magnetization in the direction of the label shift. This leads to an orthogonal movement of the magnetic vortex core, which in turn results in significant resistance changes, if the label will be shifted parallel or antiparallel to the pinning direction of the fixed layer magnetization. As outlined in figure 3(b), label shifts parallel or antiparallel to the pinning direction lead to voltage changes up to 0.4 mV. It is confirmed that the amount of the voltage change highly depends on the distance z between the label and the sensor. In this regard, a label distance of $z = 10$ nm placed at position $\Delta x = -50$ nm leads to a maximum sensor voltage of $u \approx 27.8$ mV. In contrast, a label shift parallel to the pinning direction of the fixed layer provokes a minimum voltage of $u \approx 27.1$ mV.

3.2. Label activation with out-of-plane vortex field

The present technological advances achieve saturation fields of superaramagnetic labels close to 100 mT [39–42]. Recently, some theoretical investigations on so-called Heusler alloys offer label structures that saturate at significant lower magnetic fields [20, 43]. Apart from the low-noise character, magnetic vortex structures may

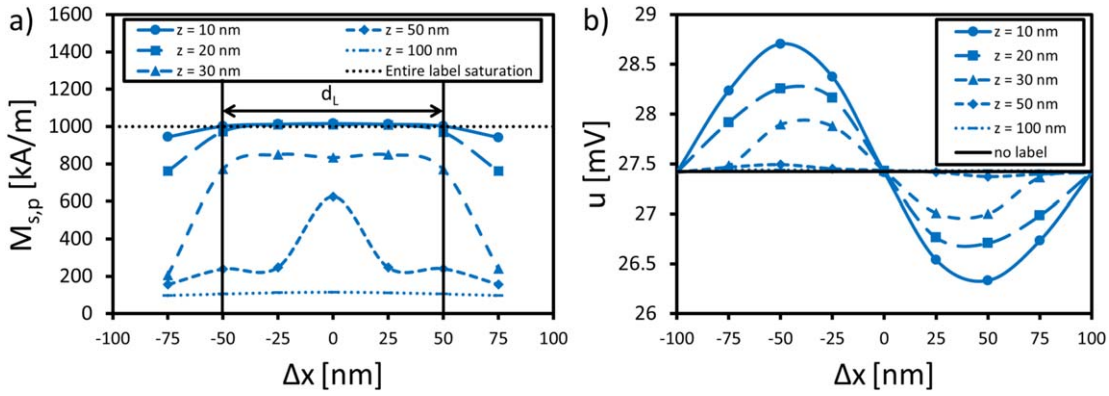

Figure 4. Simulated detection of Heusler alloy labels exploiting the out-of-plane vortex field. (a) Saturation magnetization in the label that is achieved by the stray field of the vortex depending on different in-plane label positions. Note that the lines connecting the points are interpolated. They serve as eye guides only and do not represent simulation results. (b) Simulated electric potential u of the GMR spin-valve stack for Heusler alloy labels. In both plots, the distance z is varied.

also offer the possibilty to exploit the out-of-plane vortex field for the activation of the superparamagnetic label. In this context, the saturation field of the labels should not exceed a few mT since the out-of-plane field rapidly decays in the z-direction [44]. Provided that it will be possible to design labels with such small saturation fields, the simulations in figure 4 imply that certain label positions can be saturated entirely above the vortex structure, and certain positions not. Here, we switched off the external magnetic field and simulated different label positions above the sensor structure using the Langevin function of the Heusler alloy according to figure 2(b). For this purpose, we used a label with a diameter of $d_p = 60$ nm and extracted the Langevin function using [20].

According to figure 4(a), the horizontal and the vertical distance to the vortex core as well as the distance between the label and the sensor affect the label saturation significantly. In particular, complete label saturation can be achieved when it is placed just above the vortex core or is slightly offset from it in the horizontal plane. Here, figure 4(a) indicates that a label shift of $\Delta x = 75$ nm and $\Delta y = 75$ nm in the negative and positive direction is out of the entire saturation range. Additionally, labels placed at positions $\Delta x = \pm 50$ nm and $\Delta x = \pm 25$ nm can be only saturated at a distance of $z = 20$ nm. This suggests that the distance z between the label and the sensor plays a central role. Due to the abrupt drop of the out-of-plane vortex field examined in [45], superparamagnetic labels are only saturated entirely up to a certain distance.

Concerning the sensor response shown in figure 4(b), labels placed close to the center above the sensor can be potentially better saturated but not necessarily better detected. This is due to the fact that the enormous sensor response is indicated at position $\Delta x/\Delta y = 50$ nm since labels at this position provoke the maximum magnetization change in the free layer. At this point, the sensor reacts more strongly with a maximum voltage change of $u \approx 1.3$ mV since the labels based on Heusler alloys are proposed to have a higher saturation magnetization [20, 43].

4. Discussion

In the context of micromagnetic modeling, the introduced extended model enables simulating the detection of superparamagnetic labels that are characterized by the Langevin function. As demonstrated by our simulations, this can be exploited to calibrate experimental label data directly into a LLG simulation to compute the label's effect on the sensor response of a typical GMR sensor structure. Therefore, the model offers a suitable alternative to micromagnetic simulations where labels are initially assumed ot be saturated by an external field [17]. Moreover, the model considers the effect of the out-of-plane vortex field on the label placed close to the sensor surface. In this context, the activation of superparamagnetic labels exploiting the out-of-plane vortex field is currently just a theoretical consideration. Although some publications propose nanolabels that exhibit very low saturation fields [20, 43], most state-of-the-art labels are saturated at criticals fields $h_c \geqslant 100$ mT. In perspective to the development of such low saturable nanolabels the activation by the vortex out-of-plane field is only possible with restrictions. It is found that the entire saturation of superparamagnetic labels above the sensor using the out-of-plane vortex field highly depends on the position of the label. As introduced by [44], the out-of-plane vortex field is only usable up to a certain height. Hence, in our simulation setup, only labels placed at a distance of $z \leqslant 20$ nm can be entirely saturated. However, changing the material parameters and the aspect ratio of the magnetic vortex structure is possible to manipulate the nature of the out-of-plane field. As experimentally demonstrated in [46], the strength of the out-of-plane field rises, increasing the diameter of the circular vortex

layer. Additionally, horizontal extent of out-of-plane vortex field can be enlarged by increasing thickness of the free layer [12], which offers a tantalizing perspective of fine-tuning position precision tolerance for a successful detection of superparamagnetic label by tailoring GMR sensor geometry.

One of the principal results of our simulations consists in a prediction that significant voltage changes can be produced by the GMR sensor when the label is located at a fixed distance from the free layer, moving in the plane parallel to its surface. Although this limits the detection opportunities of a single sensor element, an entire sensor array may consist of several GMR elements and fixed layers might be arranged to align in different directions. This should prevent an overlooking of a passing label and improves the reliability of the label detection.

Noise of the sensor structure is a limiting factor as well. Even though the impact of noise rises for small sensor structures, magnetic vortex structures prevent the appearance of phase noise. Hence, the noise model obtained for vortex structures considers only the contributions of the $1/f$ noise and the thermal noise [47]. As the detection of bio-functionalized labels is assigned to the low-frequency range, the $1/f$ noise becomes dominant, and the noise amplitude can be estimated by $u \approx 104$ nV [17]. This indicates an acceptable signal-to-noise ratio concerning a sensor response in the range of 27.1 mV to 27.8 mV. The amount of the simulated sensor response is consistent with already existing theoretical and experimental work in the field of nanolabel detection. Using spin-valve stripes, a single magnetite label with a diameter of $d_p = 16$ nm resulted in a resistance change of 20 mΩ [48]. Furthermore, the detection of multiple nanolabels is studied in [49] and [50], where the label is noticed through resistance and voltage changes of 100 mΩ and 90 mV, respectively. Another experimental setup for the detection of multiple magnetite nanolabels was reported in [51]. Here, a GMR Wheatstone bridge generates a response of around 5 mV for nanolabels with an average diameter of $d_p = 20$ nm. Hence, the simulated sensor response obtained in our simulations agrees well with the existing literature data, although the physics behind magnetic vortex structures is different from that used in the common GMR detection.

5. Conclusion

In conclusion, we have extended the numerical model for the low-noise GMR vortex detection of a superparamagnetic label. The extended model allows calibrating the characteristic Langevin function into the simulations and considering the effect of the free layer's stray field on the superparamagnetic label when it is placed close to the sensor surface. The use of out-of-plane vortex core field for saturation of superparamagnetic labels can be tackled only with theoretical analysis or numerical simulations for the moment, because experimental study of such systems is still hampered by the need of developing labels that can be saturated with very low fields of a few mT. The simulated sensor response is consistent with already reported theoretical and experimental investigations performed for different GMR technologies. In a nutshell, the presented model is able to consider the superparamagnetic activation through external fields more precisely and the presented GMR vortex sensor offers the possibilty for a reliable electronic readout of the label position.

Acknowledgments

The authors would like to thank the University of Kassel for funding this project.

Data availability statement

The data that support the findings of this study are available upon reasonable request from the authors.

ORCID iDs

Lukas Wetterau https://orcid.org/0000-0002-6601-4849
Claas Abert https://orcid.org/0000-0002-4999-0311
Dieter Suess https://orcid.org/0000-0001-5453-9974
Manfred Albrecht https://orcid.org/0000-0002-0795-8487

References

[1] Park J, Han D H and Park J K 2020 *Lab Chip* **20** 1191–203
[2] Sachdeva S, Davis R W and Saha A K 2021 *Front. Bioeng. Biotechnol.* **8** 1537
[3] Li H and Steckl A J 2018 *Anal. Chem.* **91** 352–71
[4] Khizar S, Ben Halima H, Ahmad N M, Zine N, Errachid A and Elaissari A 2020 *Electrophoresis* **41** 1206–24

[5] Zheng C et al 2019 IEEE Trans. Magn. 55 1–30
[6] Cao Q, Li Z, Wang Z, Qi F and Han X 2018 J. Phys. D. Appl. Phys. 51 195002
[7] Zhang S, Wang Y, Onck P and den Toonder J 2020 Microfluid Nanofluidics 24 1–20
[8] Giouroudi I and Hristoforou E 2018 J. Appl. Phys. 124 030902
[9] Lin G, Makarov D and Schmidt O G 2017 Lab Chip 17 1884–912
[10] Suess D et al 2018 Nat. Electron. 1 362–70
[11] Abert C 2019 Eur. Phys. J. B 92 120
[12] Guslienko K Y 2008 J. Nanosci. 8 2745–60
[13] Gloag L, Mehdipour M, Chen D, Tilley R D and Gooding J J 2019 Adv. Mater. 31 1904385
[14] Papaefthymiou G C 2009 Nano Today 4 438–47
[15] Ennen I, Kappe D, Rempel T, Glenske C and Hütten A 2016 Sensors 16 904
[16] Oniciuc E, Stoleriu L and Stancu A 2014 J. Magn. Magn. Mater. 352 99–106
[17] Wetterau L, Abert C, Suess D, Albrecht M and Wetterau L 2020 Sensors 20 5819
[18] Gilbert T L 2004 IEEE Trans. Magn. 40 3443–9
[19] Li Q, Kartikowati C W, Horie S, Ogi T, Iwaki T and Okuyama K 2017 Sci. Rep. 7 1–7
[20] Wegener M, Ennen I, Walhorn V, Anselmetti D, Huetten A and Dietz K J 2019 Nanomaterials 9 585
[21] Abert C, Ruggeri M, Bruckner F, Vogler C, Manchon A, Praetorius D and Suess D 2016 Sci. Rep. 6 16
[22] Aftab S, Shah S A, Nadhman A, Kurbanoglu S, Ozkan S A, Dionysiou D D and Shukla S S 2018 Int. J. Pharm 540 132–49
[23] Arias L S, Pessan J P, Vieira A P M, De Lima T M T, Delbem A C B and Monteiro D R 2018 Antibiotics 7 46
[24] Bilal M, Zhao Y, Rasheed T and Iqbal H M 2018 Int. J. Biol. Macromol. 120 2530–44
[25] Bulte J W 2019 Adv. Drug Deliv. Rev 138 293–301
[26] Dadfar S M et al 2020 J. Nanobiotechnol. 18 1–13
[27] Yamamuro S and Tanaka T 2018 J. Ceram. Soc. Jpn. 126 152–5
[28] Tang Y et al 2016 RSC Adv. 6 62550–5
[29] Anthony J W, Bideaux R A, Bladh K W and Nichols M C 2001 Handbook of Mineralogy 4 333
[30] Verba R V, Navas D, Hierro-Rodriguez A, Bunyaev S A, Ivanov B A, Guslienko K Y and Kakazei G N 2018 Phys. Rev. Appl. 10 31002
[31] Goiriena-Goikoetxea M, Guslienko K Y, Rouco M, Orue I, Berganza E, Jaafar M and Asenjo A 2017 Nanoscale 9 11269–78
[32] Martinez-Perez M J, Müller B, Lin J, Rodríguez L A, Snoeck E, Kleiner R, Sesé J and Koelle D 2020 Nanoscale 12 2587–95
[33] Metlov K L and Lee Y 2008 Appl. Phys. Lett. 92 112506
[34] Tondra M, Porter M and Lipert R J 2000 J. Vac. Sci. Technol. A 18 1125–9
[35] Liu X X and Morisako A 2008 J. Appl. Phys. 103 7E726
[36] Taslimi H, Sohi M H, Mehrizi S and Saremi M 2015 J. Mater. Sci. Mater. Electron 26 2962–8
[37] Cecot M, Karwacki L, Skowronski W, Kanak J, Wrona J, Zywczak A, Yao L, Van Dijken S and Barnas J 2017 Sci. Rep. 7 968
[38] Matula R A 1979 J. Phys. Chem. Ref. Data 8 1147–298
[39] Wallyn J, Anton N and Vandamme T F 2019 Pharmaceutics 11 601
[40] Pineiro-Redondo Y, Banobre-Lopez M, Pardinas-Blanco I, Goya G, Lopez-Quintela M A and Rivas J 2011 Nanoscale Res. Lett. 6 1–7
[41] Sharifi Dehsari H, Ksenofontov V, Möller A, Jakob G and Asadi K 2018 J. Phys. Chem. C 122 28292–301
[42] Arsalani S, Guidelli E J, Silveira M A, Salmon C E, Araujo J F, Bruno A C and Baffa O 2019 J. Magn. Magn. Mater. 475 458
[43] Kappe D, Bondzio L, Swager J, Becker A, Büker B, Ennen I, Schroeder C and Huetten A 2020 Sensors 20 4596
[44] Breitenstein L, Lendecke P, Bohlens S, Meier G and Merkt U 2008 J. Appl. Phys. 104 083909
[45] Xiao Y and Du J 2020 J. Mater. Chem. B 8 354–67
[46] Goiriena-Goikoetxea M, Guslienko K Y, Rouco M, Orue I, Berganza E, Jaafar M, Asenjo A, Fernandez-Gubieda M L, Fernandez Barquin L and Garcia-Arribas A 2017 Nanoscale 9 11269–78
[47] Weitensfelder H et al 2018 Phys. Rev. Appl. 10 054056
[48] Li G, Sun S and Wang S X 2006 J. Appl. Phys. 99 8P107
[49] Wang S X and Li G 2008 IEEE Trans. Magn. 44 1687–702
[50] Devkota J, Kokkinis G, Berris T, Jamalieh M, Cardoso S, Srikanth H, Phan M H and Giouroudi I A 2015 RSC Adv. 5 51169–75
[51] Swastika P E, Antarnusa G, Suharyadi E, Kato T and Iwata S 2018 J. Phys. Conf. Ser. 1 012060